Parameterization of Free Carrier Absorption in Highly Doped Silicon for Solar Cells

Marc Rüdiger, Johannes Greulich, Armin Richter, and Martin Hermle

***Abstract*— Free carrier absorption (FCA) is a parasitic absorption process in highly doped silicon that might significantly reduce the amount of photons, potentially generating electron-hole pairs. Existing FCA parameterizations are mostly setup by evaluating absorption data in the range $\lambda \geq 4$ μm. If applied in the wavelength range $\lambda = 1.0$–2.0 μm, including the relevant range for silicon solar cells, most parameterizations are not appropriate to describe FCA accurately. In this paper, new parameters are presented using optical simulation on the base of experimental reflection data to enhance the quantification of FCA losses in the considered wavelength range.**

***Index Terms*— Free carrier absorption (FCA), silicon devices.**

I. Introduction

FREE carrier absorption (FCA) is a parasitic absorption process, which reduces the light intensity but does not create electron-hole pairs. Thereby, photons are absorbed by either free electrons or holes, leading to a transition between states in the same (intraband absorption) or in a different band (interband absorption, e.g., transitions between two conduction bands). Thus, the photon energy is finally lost due to thermalization processes. At photon energies close to the bandgap, FCA can effectively compete with the intrinsic absorption leading to the generation of electron-hole pairs. Although FCA in silicon (Si) can be neglected for wavelengths $\lambda < 1000$ nm in general, for longer wavelengths it can become significant, especially in regions with high carrier concentrations.

Most FCA parameterizations are setup by evaluating absorption data in the range $\lambda \geq 4$ μm and, thus, far beyond the range of $\lambda = 1.0$–2.0 μm, which is relevant for Si solar cells. Because of simplicity, the models of Schroder [2] and Green [3] are based on an elementary formula structure, assuming linearity in the doping concentration N and assuming a fixed mobility μ, which does not depend on N cf. (2). This might cause a good agreement to experimental data in the evaluated wavelength range, but can cause deviations in other considered ranges. However, Isenberg [4] figured out inconsistencies by using the model of Schroder [2] at $\lambda = 5$ μm and developed a physically more profound parameterization as given in III, based on more precise models [5], [6]. So far it is unclear which model should be used for modeling FCA effects within a wavelength range of $\lambda = 1.0$–2.0 μm.

In the following, the presented FCA parameterizations will be evaluated in the wavelength range $\lambda = 1.0$–2.0 μm by comparing the simulated optical reflection curves with a broad set of experimental data for Si samples featuring different boron (B) and phosphorus (P) diffused profiles. Comparing reflection curves enables the direct evaluation of FCA effects. In this context, parameters for the simplified model by Schroder [2] are optimized to achieve an enhanced description of the influence of FCA in highly doped Si for the considered wavelength range.

II. Theory

In classical theory covering the intraband processes [7], FCA shows a quadratic behavior in λ and linear behavior in the doping concentration N (n or p, respectively)

$$\alpha_{\mathrm{FCA,n/p}}(\lambda, N) = q^3/(4\pi^2 \varepsilon_0\, c^3 n_{Si}\, m^{*2}_{e/h}\, \mu_{n/p}) \cdot \lambda^2 \cdot N \tag{1}$$

where ε_0 is the permittivity in vacuum, n_{Si} the refractive index of Si, m^* is the effective mass, and μ the carrier mobility.

With the assumption that the material parameters, in particular $\mu(N)$, are independent on N, FCA can, thus, be written as follows:

$$\begin{aligned} \alpha_{\mathrm{FCA,n}}/\mathrm{cm}^{-1} &= C_{\mathrm{FCA,n}} \cdot \left(\frac{\lambda}{\mu\mathrm{m}}\right)^{\xi} \cdot n/\mathrm{cm}^{-3} \text{ and} \\ \alpha_{\mathrm{FCA,p}}/\mathrm{cm}^{-1} &= C_{\mathrm{FCA,p}} \cdot \left(\frac{\lambda}{\mu\mathrm{m}}\right)^{\varphi} \cdot p/\mathrm{cm}^{-3} \end{aligned} \tag{2}$$

for n-type and p-type doped semiconductors, respectively. The dimensionless coefficient $C_{\mathrm{FCA,n/p}}$ includes the constants given in (1) and the exponents ξ and φ are 2.

Schroder *et al.* [2] evaluated experimentally determined absorption coefficients α_{Si} as a function of carrier concentration for the wavelengths $\lambda = 4$, 5, and 10 μm. For these wavelengths, best agreement to the experimental data is achieved with

$$C^{\mathrm{Schroder}}_{\mathrm{FCA},n} = 1.0 \times 10^{-18} \text{ and } C^{\mathrm{Schroder}}_{\mathrm{FCA,p}} = 2.7 \times 10^{-18}. \tag{3}$$

The fits showed as well that α_{FCA} depends quadratically on λ with ξ; $\varphi = 2$ [see (2)]. Schroder *et al.* [2] mentioned, that this FCA theory might yet not be thoroughly developed.

Beyond the Schroder parameters, Green [3] introduced the following widespread and simple empirical expression, which

Manuscript received February 28, 2013; revised May 2, 2013; accepted May 6, 2013. Date of current version June 17, 2013. This work was supported in part by the German Federal Ministry of Education and Research within the framework of the project "xμ-Zellen-2" under Contract 03SF0335D. The review of this paper was arranged by Editor A. G. Aberle.

The authors are with the Fraunhofer Institute for Solar Energy Systems ISE, Freiburg 79110, Germany (e-mail: marc.ruediger@ise.fraunhofer.de; johannes.greulich@ise.fraunhofer.de; armin.richter@ise.fraunhofer.de; martin.hermle@ise.fraunhofer.de).

Color versions of one or more of the figures in this paper are available online at http://ieeexplore.ieee.org.

Digital Object Identifier 10.1109/TED.2013.2262526

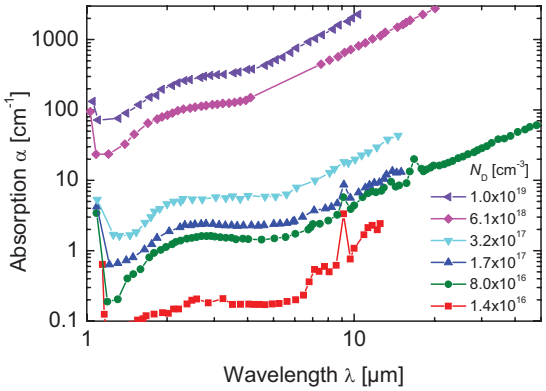

Fig. 1. Absorption coefficient as a function of wavelength for six different n-type silicon samples at room temperature (data from [1]).

is also the default FCA model in PC1D [8], for photon energies $h\nu > 0.5$ eV ($\lambda < 2.5$ μm) and charge carrier densities $\sim 10^{18}$ cm^{-3}

$$C_{\mathrm{FCA},n}^{\mathrm{Green}} = 2.6 \times 10^{-18} \quad \text{and} \quad \xi = 3$$
$$C_{\mathrm{FCA},p}^{\mathrm{Green}} = 2.7 \times 10^{-18} \quad \text{and} \quad \varphi = 2 \tag{4}$$

approving the results of Schroder for p-type Si, but showing for n-type Si a different coefficient and a cubic behavior of $\alpha_{\mathrm{FCA,n}}$ with λ ($\xi = 3$) [see (2)]. The cubic behavior follows from the evaluation of experimentally determined absorption coefficients [1] of doped n-type Si material, shown in Fig. 1. In heavily doped Si material, a linear region can be seen for $\lambda > 5$ μm, due to intraband FCA [3], featuring approximately a quadratic behavior of the wavelength. At 2 μm $< \lambda <$ 4 μm a characteristic hump appears at all considered doping levels, due to interband transitions within the two lowest conduction bands crossing at the wave vector $\mathbf{X}$ in the band structure of crystalline Si [3]. No hump appears for transitions within the valence band, i.e., for FCA due to holes in p-type Si material. Associated with this hump, an additional structure occurs for 1.2 μm $< \lambda <$ 2 μm, also due to intervalence band transitions [9]. Thus, Green [3] evaluated an approximately cubic dependence of $\alpha_{\mathrm{FCA,n}}$ on λ (i.e., $\xi = 3$).

Despite proposed more precise models [5], [6] for the dependence of the contribution of free carriers to the absorption coefficient α_{FCA}, former FCA parameterizations found more widespread application, because of their simplicity. Isenberg and Warta [4] quantified deviations of the Schroder parameterization and discrepancies of up to half an order of magnitude for an appropriate description of FCA for heavily doped layers. Based on the semiclassical approach of literature [5] valid for a range of wavelengths, they proposed a parameterization based on data at $\lambda = 5$ μm for the wavelength range from 1.2 to 8 μm

$$C_{\mathrm{FCA,n/p}}^{\mathrm{Isenberg}} = C_{\mathrm{FCA,n/p}}(\lambda) \cdot N/\mathrm{cm}^{-3} \cdot \left(\frac{\lambda}{\mu\mathrm{m}}\right)^2 \cdot \left(1 + A\left[1 + \mathrm{erf}\left\{m \log\left(\frac{N}{N_0}\right)\right\}\right]\right). \tag{5}$$

Thereby, the dimensionless carrier absorption coefficient C_{FCA} is a function of λ. A and m are dimensionless fit parameters describing the deviation of the function $\alpha_{\mathrm{FCA}}(N)$ from a linear model and N_0 is a carrier concentration used for normalization. The parameters for $\lambda = 1.2$ μm, used in this paper, were given in [4].

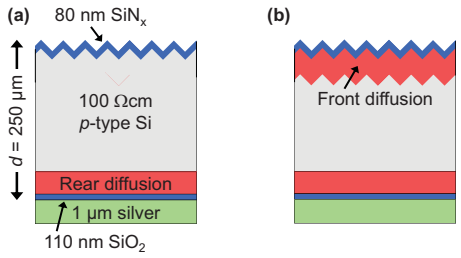

Fig. 2. Schematic sketch of the test samples produced for the analysis of free carrier absorption losses. Two variations are set up. (a) Only the rear side is diffused. (b) Front and rear side feature the same diffusion profile. The used boron and phosphorus profiles are shown in Fig. 3.

As the focus of this paper are the parameterizations of FCA, further important work covering different aspects of FCA as the band structure, gap shrinkage and the role of impurities shall be mentioned only [10]–[12].

In conclusion, it can be noticed that all published free carrier studies presented in this paper are based on the evaluation of experimental absorption data. Schroder [2] determined his parameterization with experimental data at $\lambda = 4$, 5, and 10 μm, far beyond the range of interest of $\lambda = 1.0$–2.0 μm. In the wavelength range of interest, parasitic absorption processes can occur competing with the intrinsic band-to-band absorption in highly doped Si material. In addition the parameterization of Isenberg [4] is based on data at $\lambda = 5$ μm, even though parameters are given for $\lambda = 1.2$ μm. Only the parameterization for n-type Si of Green [3] is evaluated at the range $\lambda = 1.2$–2 μm, in accordance with the wavelength range considered in this paper.

In the following, we present a comparison and detailed discussion of the above introduced models in the range of $\lambda = 1.0$–2.0 μm for reflection measurements on wafers with diffused doping profiles, evaluated with a comprehensive optical model. A new parameterization valid in this range is derived.

III. Sample Preparation

To evaluate the influence of FCA through reflection measurements, test samples are produced on 100 Ωcm p-type float zone Si base material, as shown in Fig. 2. The samples feature a thickness of 250 μm and are textured on the front side through a lithographic process with inverted pyramids to increase the effect of FCA by extending the path length of the incident light. Additionally, a precisely defined surface is achieved, enhancing the accuracy of numerical simulation of the structure. An 80-nm thick SiN_x anti-reflection layer is deposited through plasma enhanced chemical vapor deposition at the front side, while at the shiny etched planar rear surface, 110-nm SiO_2 are thermally grown. On top of the SiO_2 layer at the rear side, a 1-μm silver layer is thermally evaporated to achieve a high internal reflection to further extend the optical path length. Although four samples did not receive any diffusion and act as reference for the numerical simulations,

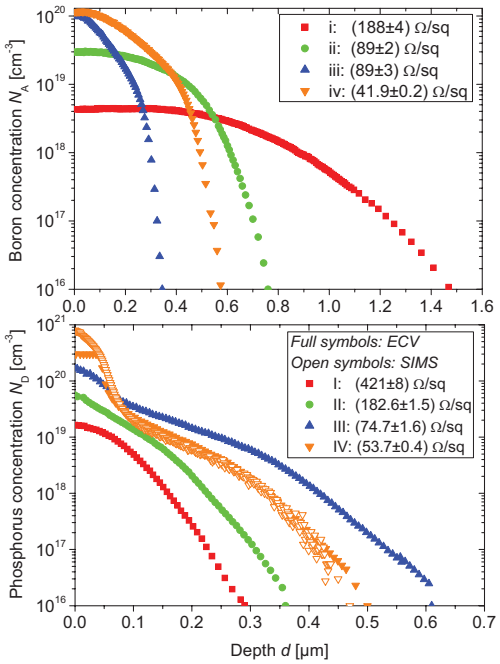

Fig. 3. Boron (top) and phosphorus (bottom) diffusion profiles used for the evaluation of FCA losses. The profiles are measured through ECV (closed symbols) and SIMS (open symbols), which only refer to phosphorus profile IV.

the rest of the samples feature different boron and phosphorus diffused profiles covering a broad range of different sheet resistances. Two different sample structures are fabricated: 1) only the rear side is diffused and 2) front and rear side feature the same diffusion profile. Using diffused doping profiles instead of samples with constant doping potentially reduces the accuracy of the FCA calculations. On the other hand, this setup with diffused profiles is the relevant one for solar cells based on crystalline silicon.

The diffusion profiles used are shown in Fig. 3. The sheet resistance values R_{sh} are the mean of two or three four-point probe measurements at different positions of the planar sample side, and are given together with their standard deviation of the mean. To avoid measurement uncertainties because of the high-low-high junction structure of both-sided B diffused samples, only one-sided diffused samples are measured. The profiles are measured by electrochemical capacitance–voltage (ECV) measurements, using a WEP-CVP21 profiler and a diluted ammonium biflouride (NH_4HF_6) electrolyte [13]. Because the first three to five measurement points of ECV measurements in general show parasitic influences and do not reflect the real doping concentration, the profile curves are extrapolated exponentially to the surface. As in ECV measurements the electrically active concentration of B and P diffusion profiles is detected, the P doping profile (IV) with a very high surface concentration above the solubility limit of 3×10^{20} cm^{-3} [14], [15], shown in Fig. 3 (below, open symbols), is measured additionally with secondary ion mass spectroscopy (SIMS) for comparison. Within a profile depth of $d = 0$–50 nm, the gap of electrically active and total P concentration, measured by SIMS, can be clearly seen. An analytical calculation of R_{sh} of profile (IV) leads to $R_{sh,ECV}(IV) = 54.7$ Ω/sq for the ECV measured profile, which is in acceptable accordance to the measured value of $R_{sh,meas}(IV) = 53.7$ Ω/sq. For the SIMS measured profile, the analytical calculation yields $R_{sh,SIMS} = 50$ Ω/sq, as expected below the measurement. For all these calculations, the mobility model by Klaassen [16], [17] is used. As FCA depends on the electrically active carrier concentration, the ECV measured profile is used for the calculations.

IV. Simulation Setup

To evaluate the influence of FCA absorption resulting from different B and P doping profiles (Fig. 3), the sample structure is setup in a numerical device simulator. A 3-D structure, setup with Sentaurus Device [18], is used to track the light paths within the Si material through a raytracer. This is able to consider an implemented arbitrary functional behavior of α_{FCA}. The 80-nm thick SiN_x anti-reflection coating is simulated via the transfer matrix method, to consider wave optical effects. The refractive index of SiN_x is determined by spectral ellipsometry from planar reference samples. In the analyzed spectral range, the applied refractive index of SiN_x varies only slightly from $n = 2.02$ at $\lambda = 1$ µm to $n = 2.01$ at $\lambda = 2$ µm. Absorption within the SiN_x thin film occurs only for $\lambda < 0.5$ µm. In the Si bulk, the Lambert-Beer law [19] is applied. A boron base doping concentration of $N_A = 1.34 \times 10^{14}$ cm^{-3} is applied, which corresponds to 100 Ωcm p-Si bulk material. The measured doping profiles are applied to each face of the inverted pyramids. This constitutes an idealization, as the diffusion at the edges of the inverted pyramids is probably different compared with a flat surface. However, as the pyramids are rather large (18.5 × 18.5-µm base area), the influence of the edges is rather small. At the rear side of the sample structure, the Phong model [20], [21] is used to describe the slight surface roughness of the shiny etched rear surface. The complex refractive index of Si is taken from [22]. As shown by Isenberg and Warta [4], the change of the real part n of the refractive index of Si because of free carriers in the doping (10^{15} to 10^{21} cm^{-3}) and the spectral range (1 µm $< \lambda <$ 2 µm) treated is smaller than 15%, which is neglected, compared with the change of its imaginary part k by several orders of magnitude.

The rear side of the numerical simulation setup has to be calibrated, as this is the only unknown set of free parameters. This is done through a reference sample, which does not have any doping diffusion and, thus, features a very high measured $R_{sh,ref} = (4000 \pm 300)$ Ω/sq. The measured spectral reflectance of the reference sample is shown for the wavelength range $\lambda = 1.0$–2.0 µm in Fig. 4 (black line). With a Phong coefficient $\omega = 800$ and a reflection rate of $R = 0.990$ at the rear side of the sample, excellent agreement with the measured reflectance could be achieved, as can be seen in Fig. 4 (black dashed line). This setup is used for all simulations presented in this paper. The simulation of the reference sample is independent of the used FCA model, as FCA does not have any effect on the very lowly doped 100-Ωcm bulk material. In the following simulation results, only the FCA models are varied.

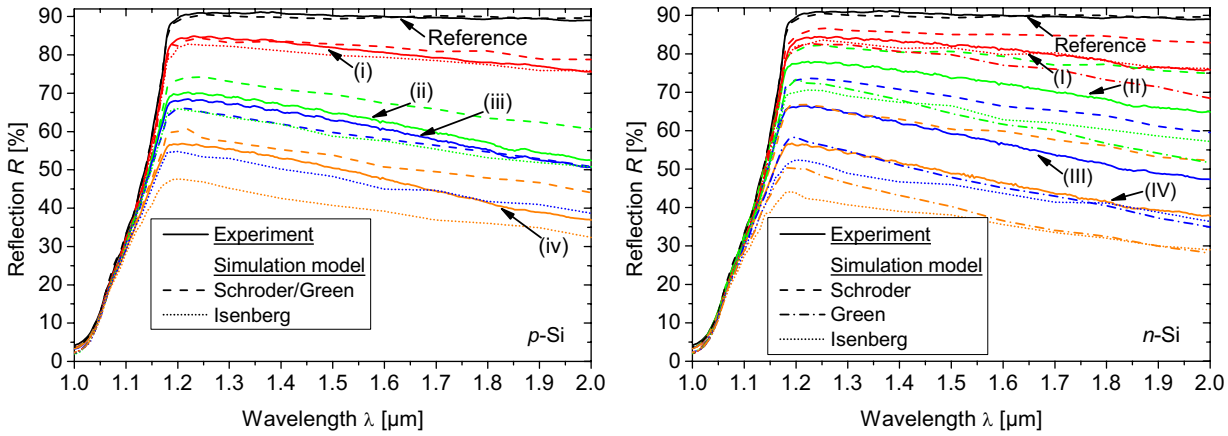

Fig. 4. Comparison of experimentally determined and calculated reflection curves for samples featuring different boron (left) and phosphorus (right) diffusion profiles. The profiles can be seen in Fig. 3, which can be identified by the Roman numerals. The influence of FCA is calculated with the models of Schroder, Green, and Isenberg. Results are shown for test samples featuring only rear side diffusions [see Fig. 2(a)].

V. Comparison of Existing Parameterizations

In the following, a comparison of simulated reflection data using the existing FCA parameterizations to experimentally determined reflection data is presented. The spectrally resolved reflectance is measured by a spectral photometer Cary500i from Varian. The measured sample is illuminated by a monochromatic light beam and the reflected light is detected by a lead sulfide photodiode. To consider the diffuse reflected light as well, the sample is placed in a highly reflective Ulbricht sphere, covered with the diffuse reflecting material polytetrafluoroethylene, commercially known as Teflon. Before each measurement, for calibration reasons, a baseline measurement without sample and a measurement with a white standard are performed.

As the test samples feature textured surfaces, light coupled into the samples passes a certain lateral distance until it might be coupled out again after multiple internal reflections. This effect could potentially lead to underestimated reflectance, as light could leave the sample outside the measurement area. To quantify this potential reflection loss, the fraction of illuminated to measured area is varied from 0.02–0.5, more precisely the illuminated area is varied by changing the aperture of the incident light beam. Thereby, no difference in the reflection data could be observed, indicating no reflection losses by this effect. For the presented measurements, an illumination fraction of 20% is used.

The optical spectroscopy is performed by a Fourier-spectrometer with detectors sensitive to wavelengths between 400 and 2200 nm. Cross check reflection measurements are performed at a second reflection measurement setup using a Fourier transformation spectrometer, allowing the measurement of the hemispheric and the diffuse part of the reflectance. The measurements yield the same results within an error of $\sim$1% absolute of the reflectance and, thus, confirming the correctness of the measurements.

A. FCA in Boron-Doped Regions

In Fig. 4 (left), the reflection measurements of the reference sample (black line) and of the test samples with the corresponding boron diffusion profiles (colored lines), given in Fig. 3 (top graph), are shown. Results are exemplarily shown for test samples featuring diffusions at the rear side cf. Fig. 2(a). The results of samples featuring diffusions at the front and rear side will be discussed as well, but are not shown explicitly. Here and in the following figures of this paper, the indication p-Si and n-Si denote the doping type of the diffusion profile, whereas the base doping type is not changed.

Results calculated with the Schroder model for the rear side diffused samples (Fig. 4, left, dashed lines) and for the both-sided diffused samples (not included) show good agreement to the experimental data in the range $\lambda = 1.0$–1.2 μm. However, it can be noticed, that the slope of calculated data for one-sided and both-sided diffused samples in the range $\lambda = 1.2$–2.0 μm are slightly different from the experimental data, leading to an increasing mismatch toward $\lambda = 2.0$ μm. Having a look at the reflectance results based on the Isenberg model (Fig. 4, left, dotted lines), it can be observed that this model tends to result in an overestimation of FCA at $\lambda \approx 1.2$ μm. With increasing FCA influence, the deviation of the slope within simulation and experiment at $\lambda > 1.2$ μm increases.

B. FCA in Phosphorus-Doped Regions

In Fig. 4 (right), the experimentally determined spectral reflectances (solid lines) are shown exemplarily for the samples featuring different phosphorus diffusion profiles, shown in Fig. 3 (bottom graph), for one-sided diffused samples cf. Fig. 2(a). Results for the both-sided diffused samples are discussed, but not shown explicitly. The calculated results feature the FCA models according to Schroder, Green, and Isenberg.

For samples with P-doped diffusion profiles the Schroder model underestimates the influence of FCA by far (5%–20% abs. reflectance difference) as shown in Fig. 4 (right). The Green model tends to overestimate the influence of FCA for most profile configurations, yielding a difference to the experimental data by $\sim$10% absolute. The Isenberg model significantly overestimates the effect of FCA for the samples with profiles (II)–(IV) in the considered wavelength range even more than the Green model.

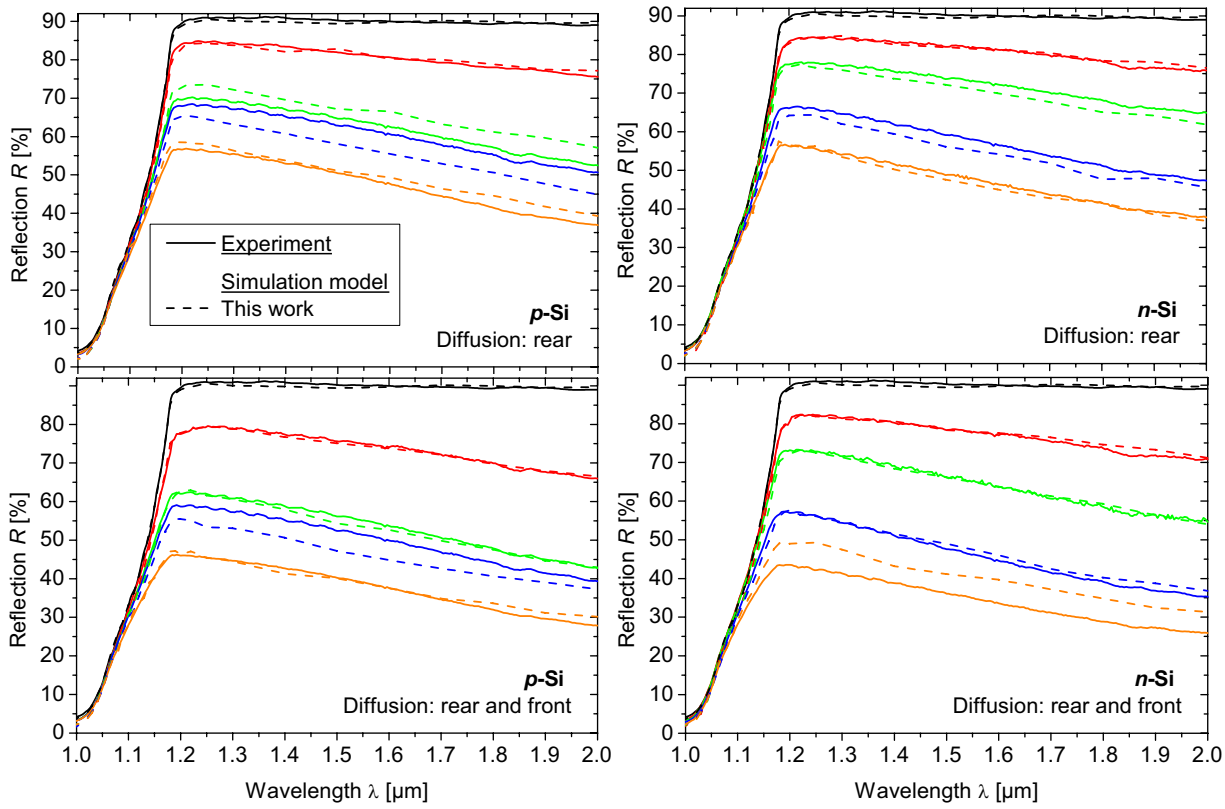

Fig. 5. Comparison of experimentally (solid lines) determined and calculated (dashed lines) reflection curves for samples featuring different boron (left) and phoshorus (right) diffusions profiles, which can be seen in Fig. 3. The influence of FCA is calculated with the set of parameters given in (7).

While the slopes of the calculated results from the Schroder and the Isenberg model feature the behavior with a slightly lower slope than observed in the experimental data, the slope of the calculated results using the Green model tends to be slightly too high because of the cubic behavior in wavelength [see (4)].

VI. Discussion

We conclude from the evaluated data shown in Fig. 4 that the simulations featuring the FCA parameterizations from literature give deviating results. Whereas the results calculated with the Schroder model for the B diffused samples are in fairly good accordance with the experimental data, simulations with the Isenberg model overestimate the influence of FCA in the considered wavelength range. For the calculations of the samples with P diffusion profiles, the Green model appears to describe the influence of FCA best within the considered models, even though a resulting difference within experimental data and simulations of ∼10% occurs. Calculation results with the Schroder model underestimate the effect of FCA, whereas with the Isenberg model the influence of FCA is again significantly overestimated. Although the Isenberg model is the parameterization based on the most enhanced physical model, it does not seem to be appropriate in the wavelength range considered in this paper. However, calculations with all presented parameterizations show deviations of the slope in the wavelength range $\lambda = 1.2$–$2.0\ \mu$m because of the different exponential dependence of α_{FCA} on λ.

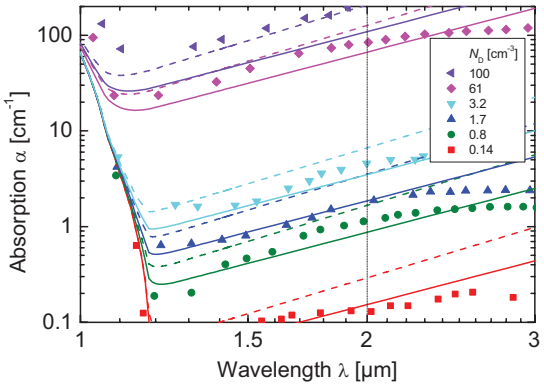

Fig. 6. Comparison of the FCA parameterization (solid lines) determined in this paper for $<2.5\ \mu$m and green parameterization (dashed lines) for $<2.5\ \mu$m, which is set up based on the shown experimental data [1] (symbols) for P-doped silicon.

Because of the observed discrepancies between the modeled and measured data for the wavelength range $\lambda = 1.2$–$2.0\ \mu$m a new set of parameters is determined. Based on the simple functional structure for the description of FCA losses, given in (2), a variation of $C_{\mathrm{FCA,n}}$, $C_{\mathrm{FCA,p}}$, ξ, and φ is set up for the entire set of data, consisting of 16 reflection curves: eight curves from the test samples featuring B diffusion profiles and eight curves from the test samples featuring P diffused profiles. For each parameter set $p' = \{C_{\mathrm{FCA,n}}, C_{\mathrm{FCA,p}}, \xi; \varphi\}$(samples with B or P doped profiles, respectively) the spectral reflectance $R_{\mathrm{sim},i}(p',\lambda)$ $(i = 1, \ldots, n')$ of all $n' = 8$ samples are

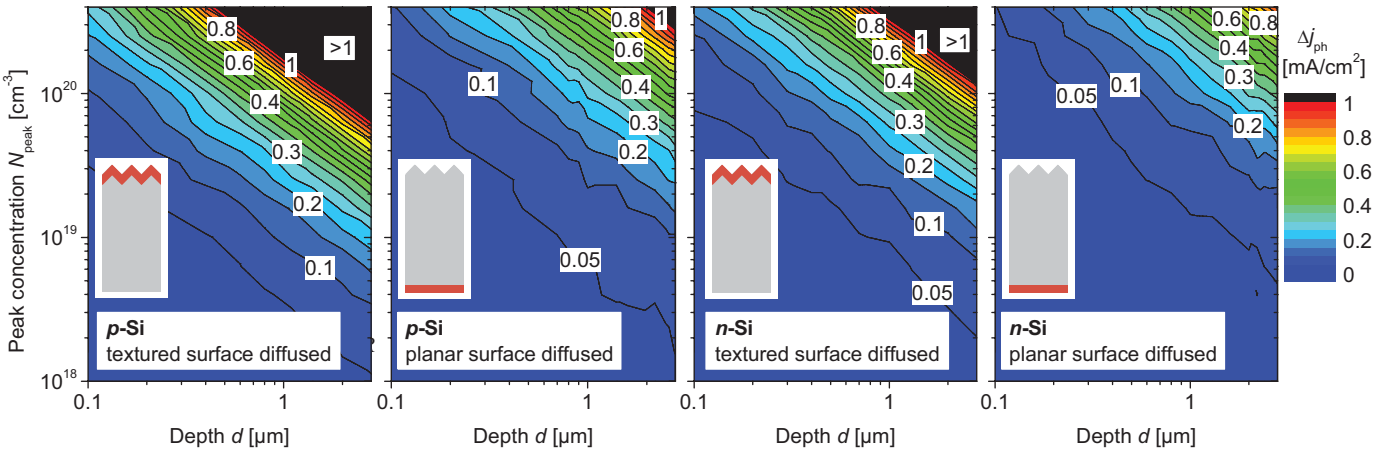

Fig. 7. Photogenerated current density losses Δj_{ph}, exemplarily shown for varied Gaussian profiles on textured and planar surfaces for B- and P-doped silicon, respectively.

simulated and the mean absolute errors maximum asymptotic efficiency (MAE) to the experimentally determined reflection curves $R_{\text{meas},i}(\lambda)$ ($i = 1, \ldots, n'$), respectively, are determined

$$\text{MAE} = \frac{1}{n'} \cdot \sum_{i=1}^{n'} \left(\frac{1}{m'} \sum_{j=1}^{m'} \left| R_{\text{sim},i}\left(p', \lambda_j\right) - R_{\text{meas,i}}\left(p', \lambda_j\right) \right| \right). \tag{6}$$

Equal weight is given to each wavelength λ_j ($j = 1,\ldots, m'$). The MAE of the entire set of data is minimized for the following set p'_{min} of parameters

$$\alpha_{\text{FCA,p}}/\text{cm}^{-1} = 2.6 \cdot 10^{-18} \cdot \left(\frac{\lambda}{\mu\text{m}}\right)^{2.4} \cdot p/\text{cm}^{-3} \quad \text{and}$$
$$\alpha_{\text{FCA,p}}/\text{cm}^{-1} = 1.8 \cdot 10^{-18} \cdot \left(\frac{\lambda}{\mu\text{m}}\right)^{2.6} \cdot n/\text{cm}^{-3} \tag{7}$$

valid for the wavelength range $\lambda = 1.0$–2.0 μm. The spectral reflectances calculated with this set of parameters are shown in Fig. 5 for the set of samples featuring B diffusions (left) and for the set of samples featuring P diffusions (right). Whereas the reflection data feature a maximum deviation of ~5% absolute within experimental and simulated data, the overall agreement is significantly enhanced. Because of the adapted exponential behavior, the slopes of the calculated data coincide very well with the experimental data, indicating an exponential behavior of the wavelength of ~2.5 for n- and p-Si in contrast to previously published assumptions.

In Fig. 6, experimental data given in literature (symbols) are plotted for Si:P in comparison with the parameterization presented in this paper (lines), and the parameterization of Green (dashed lines). As no experimental data are available for p-type Si for $\lambda < 2.4$ μm, a comparison with the present parameterization is not possible. For n-Si, a detail of the experimental data from Spitzer [1] (symbols) is shown in Fig. 6, which is an excerpt of Fig. 1. For comparison, the parameterization presented in this paper (solid lines) and the parameterization of Green (dashed lines) are plotted. It can be observed that the parameterization of Green, which is based on these experimental data, is for $N_D < 10^{18}$ cm^{-3} higher than the experimental data at $\lambda = 1.2$–2.0 μm, overestimating FCA slightly. This result is consistent with the observations made in Fig. 4 (right). Here, (7) seems to fit slightly better the experimental data. For $N_D > 10^{18}$ cm^{-3} contrary behavior can be observed, the Green model appears to fit the data best. But the experimental data for $N_D = 6.1 \times 10^{18}$ cm^{-3} and 1×10^{19} cm^{-3} might be incorrect for the following reason. At $\lambda = 1.0$–1.2 μm the measured absorption coefficient α is significantly higher in comparison with the very precise $\alpha_{\text{Si}}(\lambda)$ data for band-to-band absorption from Green [22] probably indicating an overestimation of the measured α. Thus, α_{FCA} might be overestimated for the experimental values of Spitzer for these doping concentrations. Toward high doping concentrations, deviations might be caused as well by the negligence of nonlinearity effects in n. Linear behavior in the electron concentration n is assumed in the parameterizations for both this paper [see (7)] and that of Green [see (4)]. As well for the highest doping concentration $N_D = 10^{19}$ cm^{-3} the latter parameterization predicts an absorption coefficient α_{FCA} smaller than the experimental data (for $\lambda = 1.0$–1.7 μm). A change of the real part of the refractive index at high doping concentrations might not be the reason for the deviations, as the influence is very small for $\lambda < 2$ μm. (see Fig. 3 in [4]). In addition, the use of the Phong-model is deemed to be related neither to the deviations at high doping concentrations, as very good accordance of simulated and experimentally determined reflection data of the reference sample could be achieved (see Fig. 4).

From the numerical simulation setup, the photogenerated current density loss Δj_{ph} caused by FCA can be quantified. Δj_{ph} by using (7) is exemplarily shown in Fig. 7 for varied Gaussian profiles for both, B- and P-doped Si. The standard domain is identical to the one shown in Fig. 2, but the diffusion profile is applied on the textured front or the planar rear surface, respectively (Fig. 7, insets). Because of the increased surface for textured surfaces and, thus, an increased highly doped area after diffusion, the effect of FCA is significantly

TABLE I

Δj_{ph} CAUSED BY FCA FOR THE EXAMINED DIFFUSION PROFILES GIVEN IN FIG. 3. THE LOSSES HAVE BEEN CALCULATED BY THE USE OF (7)

Profile	Dopant	Sheet resistance R_{sh} [Ω/sq]	Photogenerated Current Density Loss Δj_{ph} [mA/cm^2]	
			Textured	Planar
i	B	188 ± 4	0.1	< 0.05
ii	B	89 ± 2	0.3	0.1
iii	B	89 ± 3	0.4	0.1
iv	B	41.9 ± 0.2	0.6	0.3
I	P	421 ± 8	< 0.05	< 0.05
II	P	182.6 ± 1.5	0.1	< 0.05
III	P	74.7 ± 1.6	0.2	0.1
IV	P	53.7 ± 0.4	0.4	0.2

increased as well. The FCA losses for the examined diffusion profiles given in Fig. 3 are quantified as well and are shown in Table I. For B-doped profiles, Δj_{ph} varies between < 0.05 mA/cm^2 for the very shallowly doped profile (i) on planar surfaces, up to a significant calculated influence of $\Delta j_{ph} = 0.6$ mA/cm^2 for profile (iv) on textured surfaces. The calculations show for the considered P-doped profiles a loss range of $\Delta j_{ph} = < 0.05$–0.4 mA/cm^2. Δj_{ph} of profile (IV) is also calculated via the SIMS profile (because of measurement artifacts at the surface, the first three to four measurement points at the surface are corrected via extrapolation) instead of the ECV profile. Then the loss caused by FCA would be overestimated by 0.1 and 0.2 mA/cm^2. Thus, when SIMS measurements of P-doped profiles are included in numerical device simulations, profile concentrations above the solubility limit [14] should be corrected.

By calculating the Δj_{ph} losses shown in Table I with the Green parameterization, the same results can be observed for the B-doped profiles (iiv). For the P-doped profiles (IIV), the resulting Δj_{ph} values differ by a factor of about 0.5, which is a relevant underestimation of the effect of FCA.

The results shown in Fig. 7 and Table I indicate that FCA is a nonnegligible loss mechanism in highly doped Si, which plays an important role for an accurate description of the device current density and should be considered in device simulations.

VII. CONCLUSION

In this paper, existing FCA models were evaluated according to their validity within the wavelength range $\lambda = 1.0$–2.0 μm. This included the relevant range where FCA could potentially decrease the photogenerated current density j_{ph} in highly doped Si. Therefore, test samples were produced featuring different B- and P-doped diffusion profiles, covering a broad range of sheet resistances, and the corresponding reflection curves were measured. Based on numerical device simulations, the same test structures were simulated, including the different FCA parameterizations from Schroder [2], Green [3], and Isenberg [4]. Significant deviations of the simulated reflection curves could be observed by comparing the results of the different parameterizations found in the literature. Whereas simulations, including the Schroder parameterization for B-doped Si—which is identical to the Green parameterization for Si:B—showed fairly good agreement with the experimental data, most other simulations showed significant differences to the set of experimental data, including Si:P and Si:B, over- or underestimating the effect of FCA.

Therefore, based on the classical theory [7], new parameters for the quantification of FCA losses were set up, achieving very good agreement with the experimental data. Based on this parameterization, losses on j_{ph} due to FCA are quantified for different doping concentrations and explicitly for the investigated experimental profiles on textured and planar surfaces. The results illustrate that FCA is a nonnegligible loss mechanism in highly doped Si, which plays an important role for an accurate description of device current density losses. Because of the simplistic formula structure, the parameterization might be easily implemented in numerical simulation tools.

ACKNOWLEDGMENT

The authors would like to thank H. Hauser and B. Dimitrova for reflection measurements, and H. Hauser and C. Reichel for fruitful discussions.

REFERENCES

[1] W. Spitzer and H. Y. Fan, "Infrared absorption in the n-type silicon," *Phys. Rev.*, vol. 108, no. 2, pp. 268–271, 1957.
[2] D. K. Schroder, R. N. Thomas, and J. C. Swartz, "Free carrier absorption in silicon," *IEEE J. Solid-State Circuits*, vol. 13, no. 1, pp. 180–187, Feb. 1978.
[3] M. A. Green, *Silicon Solar Cells: Advanced Principles and Practice*. Sydney, Australia: UNSW, 1995.
[4] J. Isenberg and W. Warta, "Free carrier absorption in heavily doped silicon layers," *Appl. Phys. Lett.*, vol. 84, no. 13, pp. 2265–2267, Jan. 2004.
[5] R. A. Smith, *Semiconductors*, 2nd ed. Cambridge, U.K.: Cambridge Univ. Press, 1978.
[6] E. Conwell and V. F. Weisskopf, "Theory of impurity scattering in semiconductors," *Phys. Rev.*, vol. 77, no. 3, pp. 388–390, Feb. 1950.
[7] R. A. Smith, *Semiconductors*, 1st ed. Cambridge, U.K.: Cambridge Univ. Press, 1961.
[8] D. A. Clugston and P. A. Basore, "Modelling free-carrier absorption in solar cells," *Progr. Photovolt., Res. Appl.*, vol. 5, no. 4, pp. 229–236, Jul.–Aug. 1997.
[9] E. Barta, "Optical constants of various heavily doped p-and n-type silicon crystals obtained by Kramers-Kronig analysis," *Infr. Phys.*, vol. 17, no. 5, pp. 111–119, Sep. 1977.
[10] M. Balkanski, A. Aziza, and E. Amzallag, "Infrared absorption in heavily doped n-type Si," *Phys. Status Solidi (b)*, vol. 31, no. 1, pp. 323–330, 1969.
[11] P. E. Schmid, "Optical absorption in heavily doped silicon," *Phys. Rev. B*, vol. 23, no. 10, pp. 5531–5536, May 1981.
[12] R. A. Soref and B. R. Bennett, "Electrooptical effects in silicon ," *IEEE J. Quantum Electr.*, vol. 23, no. 1, pp. 123–129, Jan. 1987.
[13] M. Rauer, M. Rüdiger, C. Schmiga, H. Strutzberg, M. Bähr, M. Glatthaar, and S. W. Glunz, "Interpretation of recombination at c-Si/SiN_x interfaces by surface damage," *J. Appl. Phys.*, vol. 108, no. 1, pp. 014506-1–014506-9, Jul. 2010.
[14] A. Kimmerle, A. Wolf, U. Belledin, and B. Biro, "Modelling carrier recombination in highly phosphorus-doped industrial emitters," *Energy Procedia*, vol. 8, pp. 275–281, Aug. 2011.
[15] S. Solmi, A. Parisini, R. Angelucci, A. Armigliato, D. Nobili, and L. Moro, "Structural evolution of implanted vicinal Si(111) during annealing via analysis of the dipole contribution," *Phys. Rev. B*, vol. 53, no. 2, pp. 7836–7841, 1996.
[16] D. B. M. Klaassen, "A unified mobility model for device simulation—I. Model equations and concentration dependence," *Solid-State Electron.*, vol. 35, no. 7, pp. 953–959, Jul. 1992.

[17] D. B. M. Klaassen, "A unified mobility model for device simulation—II. Temperature dependence of carrier mobility and lifetime," *Solid-State Electron.*, vol. 35, no. 7, pp. 961–967, Jul. 1992.
[18] *Sentaurus TCAD*, Synopsys, Zürich, Switzerland, 2013.
[19] E. Hecht, *Optics*. Reading, MA, USA: Addison-Wesley, 2002.
[20] J. Foley, A. van Dam, S. Feiner, and J. Hughes, *Computer Graphics*. Reading, MA, USA: Addison-Wesley, 1990.
[21] B. T. Phong, "Communication of the association for computer machinery," *Comput. Sci. J.*, vol. 18, no. 6, pp. 311–317, Jun. 1975.
[22] M. A. Green, "Optical modeling of the rear surface roughness of passivated silicon solar cells," *Solar Energy Mater. Solar Cells*, vol. 92, no. 11, pp. 1305–1310, 2008.

Marc Rüdiger is currently pursuing the Ph.D. degree with the Silicon Solar Cells-Development and Characterization Division, Fraunhofer Institute for Solar Energy Systems, Freiburg, Germany.

His current research interests include analysis, characterization and modeling of crystalline silicon solar cells.

Johannes Greulich is currently pursuing the Ph.D. degree with the Division of PV Production Technology and Quality Assurance, Fraunhofer Institute for Solar Energy Systems, Freiburg, Germany.

Armin Richter is currently pursuing the Ph.D. degree with the Silicon Solar Cells-Development and Characterization Division, Fraunhofer Institute for Solar Energy Systems, Freiburg, Germany.

His current research interests include the development and characterization of silicon surface passivation with atomic layer deposited Al_2O_3 layers.

Martin Hermle received the Ph.D. degree in physics from the University of Konstanz, Konstanz, Germany, in 2008.

His current research interests include the development of solar cell technologies for high-efficiency silicon solar cells and the analysis, characterization, and modeling of silicon and III–V solar cells.